Can Luzon Strait Transport Play a Role in Conveying the Impact of ENSO to the South China Sea?*

Tangdong Qu, Yoo Yin Kim, and Max Yaremchuk

International Pacific Research Center, SOEST, University of Hawaii at Manoa, Honolulu, Hawaii

Tomoki Tozuka

Department of Earth and Planetary Science, University of Tokyo, Tokyo, Japan

Akio Ishida

Frontier Research System for Global Change, Yokohama, and Japan Marine Science and Technology Center, Yokosuka, Japan

Toshio Yamagata

Department of Earth and Planetary Science, University of Tokyo, Tokyo, and Frontier Research System for Global Change, Yokohama, Japan

ABSTRACT

The Luzon Strait transport (LST) from the Pacific into the South China Sea (SCS) is examined using results from a high-resolution ocean general circulation model. The LST from the model has a mean value of 2.4 Sv ($Sv \equiv 10^6$ m^3 s^{-1}) and reaches its seasonal maximum (6.1 Sv westward) in winter and seasonal minimum (0.9 Sv eastward) in summer. Both the annual mean and seasonal variation of LST compare favorably with earlier observations. On an interannual time scale, LST tends to be higher during El Niño years and lower during La Niña years, with its maximum (minimum) leading the mature phase of El Niño (La Niña) by 1 month. The interannual variation of LST appears to be oppositely phased with the Kuroshio transport east of Luzon, indicating a possible nonlinear hysteresis of the Kuroshio as a driving mechanism of LST. For the annual average, water leaving the SCS in the south is of higher temperature than that with LST, thus producing a cooling advection in the upper 405 m equivalent to a surface heat flux of -19 W m^{-2}. Most of this cooling advection is balanced by the atmospheric heating (17 W m^{-2}). From late spring to early fall, surface heat flux is the primary heating process; only a small part of the heat content change can be explained by heat advection. But, in winter, heat advection seems to be the only important process responsible for the cooling in the upper layer of the SCS. The interannual variation of the upper-layer heat content has a strong signature of ENSO, cooling in the development of El Niño and warming in the development of La Niña. An oceanic connection is revealed, in which LST seems to be a key process conveying the impact of the Pacific ENSO into the SCS.

1. Introduction

The South China Sea (SCS) climate is part of the East Asian monsoon system and appears to be connected with the El Niño–Southern Oscillation (ENSO) in the Pacific (e.g., Zhang et al. 1996; Tomita and Yasunari 1996; Ose et al. 1997). The connection between the SCS climate and the Pacific ENSO has become a very active area of research, primarily using atmospheric data. Among others, Wang et al. (2000) noted that the key system that bridges the SCS climate and Pacific ENSO is an anomalous anticyclonic/cyclonic circulation located in the western North Pacific. It has been known, however, that there is a water exchange between the SCS and the Pacific through the Luzon Strait (Fig. 1; Wyrtki 1961). Can this water exchange also play a role in conveying the impact of ENSO to the SCS? Until now, the oceanic connection between the SCS climate and the Pacific ENSO has only begun to be investigated (Yamagata and Behera 2001). This study represents the initial attempts to provide preliminary evidence for this oceanic connection as a background for future studies of the ocean's role in the SCS climate.
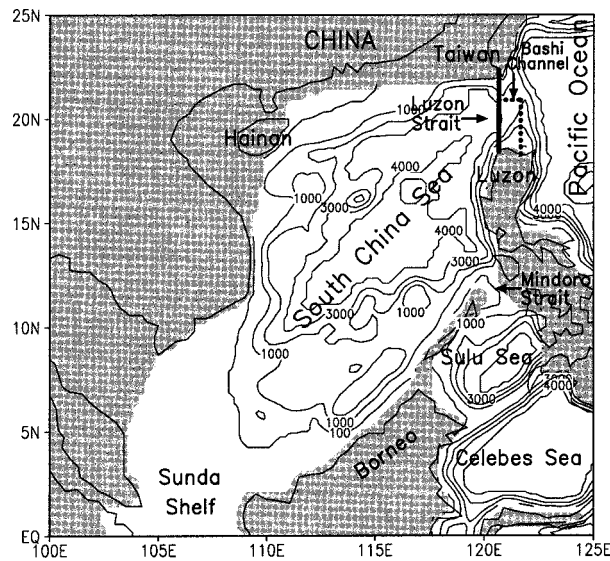
FIG. 1. Bottom topography of the South China Sea in the model derived from the ETOPO5.

The water exchange between the SCS and the Pacific through the Luzon Strait has been extensively studied in past decades. Wyrtki (1961) first noted that water enters the SCS in winter and flows back to the Pacific in summer. This is true, however, only for the surface layer, where the ocean circulation is predominantly forced by monsoonal winds. Within the depth range of the thermocline, later observations revealed that there is a Kuroshio branch flowing westward along the continental slope south of China both in winter and summer (Qiu et al. 1984; Guo 1985) and the intrusion of North Pacific tropical water seems to occur during most, if not all, seasons of the year (Shaw 1991; Qu et al. 2000).

Wyrtki (1961) also noted that the flow in Luzon Strait changes its sign at about 300 m in winter and at about 400 m in summer. Despite considerable seasonal variation, later observations (e.g., Chen and Huang 1996) suggested that the SCS water mainly flows out of the SCS through Luzon Strait at depths between 350 and 1350 m to compensate the inflow of Pacific water in the surface layer. Water mass distribution provided further evidence showing that water at intermediate depth flows in the opposite direction to that near the surface (Qu et al. 2000). This vertical structure has been well reproduced by numerical models, though the vertical extension of the outflow is slightly different with different models (e.g., Chao et al. 1996; Yuan 2002).

In the deep layer of the SCS (below 2000 m), water is relatively homogenous and appears to have the same characteristics as the Pacific water at about 2000 m (Nitani 1972; Broecker et al. 1986). This has been interpreted as evidence for Wyrtki's (1961) speculation that water enters the SCS from the Pacific around the sill depth (~2000 m) of Luzon Strait. The abyssal water transport across the Luzon Strait was estimated to be

about 0.7 Sv (Sv $\equiv 10^6$ m^3 s^{-1}) at depths 1500–2500 m (Wang 1986). Because this Pacific water is colder and of higher density, it sinks after crossing the strait and, as a consequence, the renewal of the SCS deep water is rapid compared with its western North Pacific counterpart.

The total transport through Luzon Strait, called the Luzon Strait transport (LST) hereinafter, is essentially westward. Studies of LST have arrived at mean transport estimates ranging from 0.5 to 10 Sv (e.g., Wyrtki 1961; Metzger and Hurlburt 1996; Qu 2000; Lebedev and Yaremchuk 2000; Chu and Li 2000; Qu et al. 2000; Yaremchuk and Qu 2004). With a set of numerical experiments, Metzger and Hurlburt (1996) noted that LST is particularly sensitive to the model geometry. Qu et al. (2000) applied Godfrey's (1989) "island rule" to the Philippines and interpreted LST as a result of counterbalance between the basin-scale forcing of the Pacific and the friction created in the narrow and shallow passages that connect the SCS with its surrounding oceans (Fig. 1).

For seasonal variation, a common feature of the earlier studies is that LST is larger in winter and smaller in summer in response to the seasonal reversing monsoon. Among others, Qu (2000) derived from hydrographic observations a maximum of 5.3 Sv in January–February and a minimum of 0.2 Sv in June–July, while Chu and Li's (2000) estimate is somewhat larger, with a maximum of 13.7 Sv in February and a minimum of 1.4 Sv in September. These discrepancies could be due to uncertainties in the intermediate and deep circulations. In a recent diagnostic analysis that combines atmospheric climatologies with drifter, satellite altimetry, and hydrographic data in the framework of a numerical model, Yaremchuk and Qu (2004) obtained a seasonal cycle of LST with a maximum of 4.8 Sv in January–February and a minimum of 0.8 Sv in August, showing better agreement with Qu's (2000) estimate.

There is no doubt that these earlier studies have significantly advanced our knowledge of LST. However, due to the lack of observations, the interannual variation of LST and its possible role in the SCS thermal balance remain unknown. Simply put, can LST play a role in conveying the impact of ENSO to the SCS? This study is intended to address this question using results from a high-resolution ocean general circulation model. Results of the analysis are presented in the following sections. After a brief description of the model in section 2, some general characteristics of the simulation are described in section 3. Section 4 describes LST and its variations. Section 5 examines the influence of LST on the SCS thermal balance, and results are summarized in section 6.

2. Description of the model

The model selected for this study was based on the Modular Ocean Model version 2 (Ishida et al. 1998). It

has a horizontal resolution of ¼° both in latitude and longitude and has 55 levels in the vertical whose spacing varies from 10 m near the sea surface to about 50 m in the intermediate layers and about 400 m at a 6000-m depth. The model is zonally global with its southern and northern boundaries closed at 75°S and 75°N, respectively, and has a realistic coastline and bottom topography derived from the National Geophysical Data Center's Earth Topography Five Minute (ETOPO5) dataset with a $5' \times 5'$ resolution. In the SCS, the model resolves all the shallow passages that connect the SCS with its surrounding oceans, including the Sunda shelf and Mindoro Strait, but allows no water exchange with the East China Sea at Taiwan Strait (Fig. 1). Closing Taiwan Strait (<100 m) in the model may reduce LST and possibly influence the SCS thermal balance. We will come back to this point later.

The model was spun up from the initial state at rest with annual-mean temperature and salinity from Levitus (1982). It was forced with the Hellerman and Rosenstein (1983) annual-mean wind stress during the first two model years and afterward with the Hellerman–Rosenstein monthly wind stress for 18 years. The heat and freshwater flux during these two intervals of time was implemented as a linear restoring of temperature and salinity in the first model level toward the Levitus (1982) annual mean and monthly climatologies, respectively. A highly scale-selective biharmonic operator was used for horizontal turbulent mixing, with a coefficient of -1×10^{19} cm^4 s^{-1} for both momentum and tracers, and the Pacanowski and Philander (1981) formulation was used for vertical mixing. Then, the model was further integrated for 17 years with 3-day-averaged ECMWF wind stress from January 1982 to December 1998. Sea surface temperature was relaxed to Reynolds sea surface temperature and sea surface salinity to the Levitus (1982) monthly climatology. In the deep layers, the integration of the model was apparently not long enough to spin up the deep-layer circulation. To make the deep-layer circulation diagnostically robust, a restoring with a 2-yr time scale to the Levitus (1982) annual mean temperature and salinity was included in the tracer equations below 2000 m (Ishida et al. 1998). The monthly data of the last 17 years were used for the present analysis.

3. General characteristics of the simulation

The model outputs of its seasonal run have been analyzed by several earlier studies (e.g., Ishida et al. 1998; Qu et al. 2002). These earlier studies indicated that the model has a reasonable representation of the circulation in the western Pacific, including the North Equatorial Current (NEC), the Mindanao Current, and the Kuroshio. To verify the circulation in the SCS, monthly velocity fields averaged from 1982 to 1998 are presented in this section.

In general, the model reproduces the SCS circulation pretty well. At depths of the thermocline, the intrusion of the Kuroshio water is markedly evident in Luzon Strait. Much of the Kuroshio water, however, returns to the Pacific before reaching 120°E (Fig. 2). Within the SCS, the circulation from the model shows essentially the same pattern as that from Qu (2000) based on historical temperature data, both showing a strong cyclonic circulation in winter and a weak anticyclonic circulation in summer. The West Luzon eddy and the East Vietnam eddy shown in Qu's (2000) climatology are also reproduced. Large discrepancies occur at the western boundary where narrow western boundary currents are not well resolved in Qu's (2000) climatology, presumably as a result of smoothing used in preparing his dataset. The Kuroshio South China Sea branch (KSCSB) reported by earlier studies (Qiu et al. 1984; Guo 1985) is indeed a year-round phenomenon, though its strength is season dependent. In winter, when the northeast monsoon prevails, the KSCSB extends all the way to the southwestern corner of the basin (Fig. 2), consistent with the water mass distribution presented by Qu et al. (2000). In summer, when the wind is from the southwest, the KSCSB becomes weaker. It separates from the coast around the southern tip of Vietnam. From there, part of it turns northward to join the East Vietnam eddy. To the south, the western boundary current is actually northward and seems to be related to an anticyclonic eddy around the southwestern corner of the basin (Fig. 2).

In the intermediate layer, the circulation is relatively weak, but the KSCSB is still evident in winter (Fig. 3). The cyclonic circulation forced by the northeast monsoon is primarily confined in the northern SCS, and the KSCSB separates from the coast farther northward (13°–15°N) than that in shallower waters. In summer, the KSCSB disappears in the intermediate layer and the western boundary current along the coast of Vietnam is reversed (Fig. 3). Although no observational evidence is available at this time, most of these phenomena are consistent with earlier simulations (e.g., Chao et al. 1996; Yuan 2002).

4. Luzon Strait transport

a. Annual mean

The mean LST from the model is 2.4 Sv, of which the directly wind-driven component (i.e., Ekman drift) is negligible, accounting for only about 10% of the total transport. This transport is well confined in the upper 405 m (i.e., the upper 21 layers of the model). Although water exchange does occur in the deeper layers, the net transport below 405 m is very close to zero. Since there is no Taiwan Strait in the model (Fig. 1), all water entering the SCS through Luzon Strait turns southward and exits the SCS across the Sunda shelf into the Indian Ocean (1.7 Sv) and through Mindoro Strait into the Sulu Sea (0.7 Sv) and eventually the Pacific Ocean. The annual mean streamfunction of total transport provides an overview of this circulation (Fig. 4). Mindoro Strait is
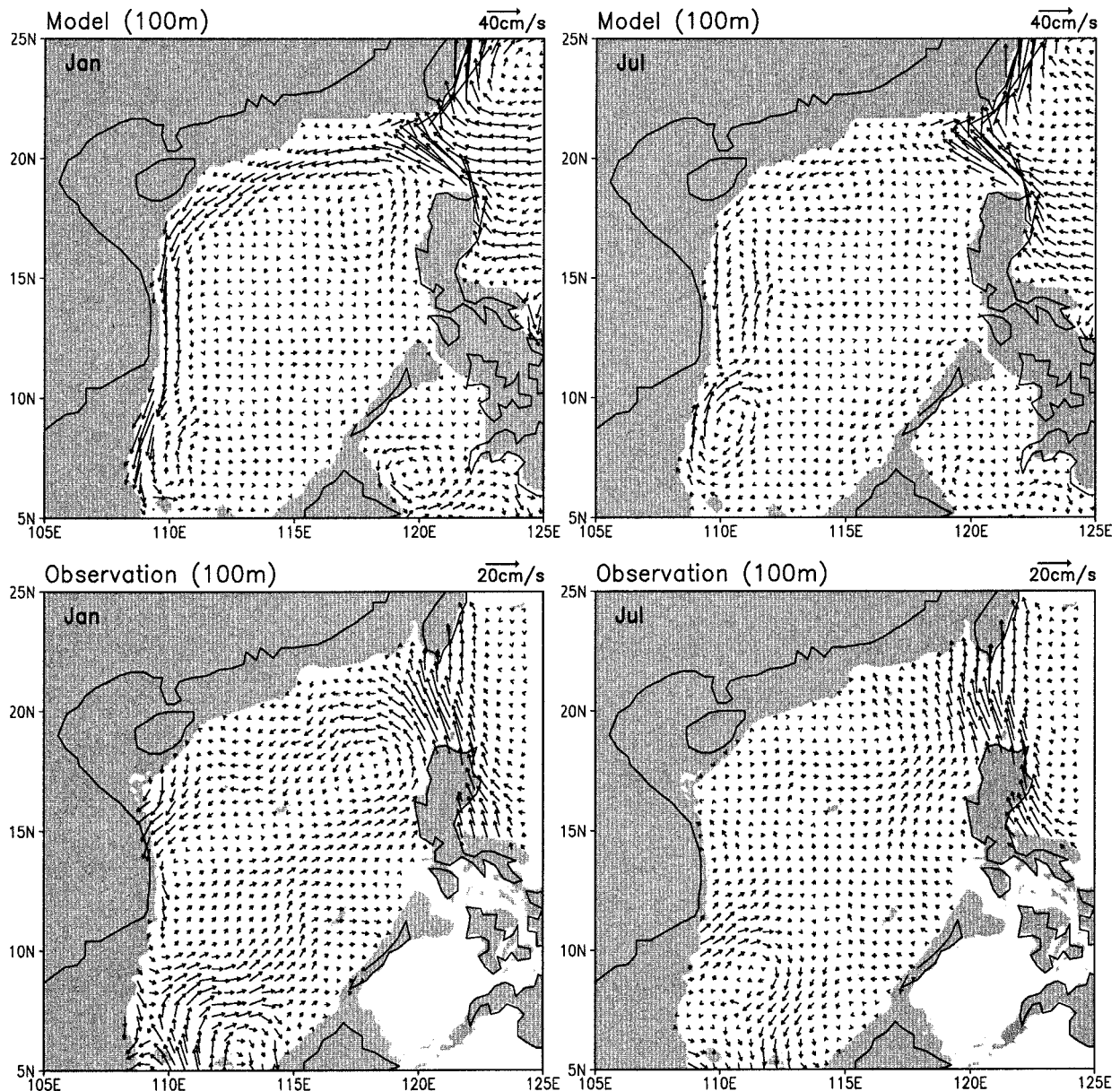
FIG. 2. Monthly mean circulation at 100 m from the model and observations (Qu 2000) in Jan and Jul.

about 120 m deep in the model, about 100 m shallower than the reality. As a result, the circulation around the Philippines is slightly weaker than suggested by Godfrey's (1989) "island rule" (Qu et al. 2000). Closing Taiwan Strait likely reduces the LST in the model. Earlier studies suggested that the Taiwan Strait transport lies between 1 and 2 Sv in the mean (Fang et al. 1991). Thus, the LST (2.4 Sv) produced by the model is relatively small, but its southward component across the Sunda shelf and through Mindoro Strait is still comparable with earlier observations and simulations (e.g., Qu 2000; Lebedev and Yaremchuk 2000).

Figure 5 shows the velocity distribution in Luzon Strait. At 120.75°E (indicated by the meridional heavy solid line in Fig. 1), where Luzon Strait is narrowest, the flow is dominated by a westward component (inflow) in the south and an eastward component (outflow) in the north (Fig. 5a). The inflow is relatively weak with a maximum speed of about 40 cm s^{-1}, but broader than the outflow by a factor of at least 2. Weak inflows/ outflows are also evident in the deeper layers, say, below 1500 m, indicative of an exchange of abyssal water between the SCS and the Pacific. At 121.75°E (indicated by the meridional heavy dotted line in Fig. 1) where water depth is generally shallower than 2000 m, much of the inflow along the southern part of the section (Fig. 5b) turns northward and exits the SCS through the Bashi Channel (indicated by the zonal
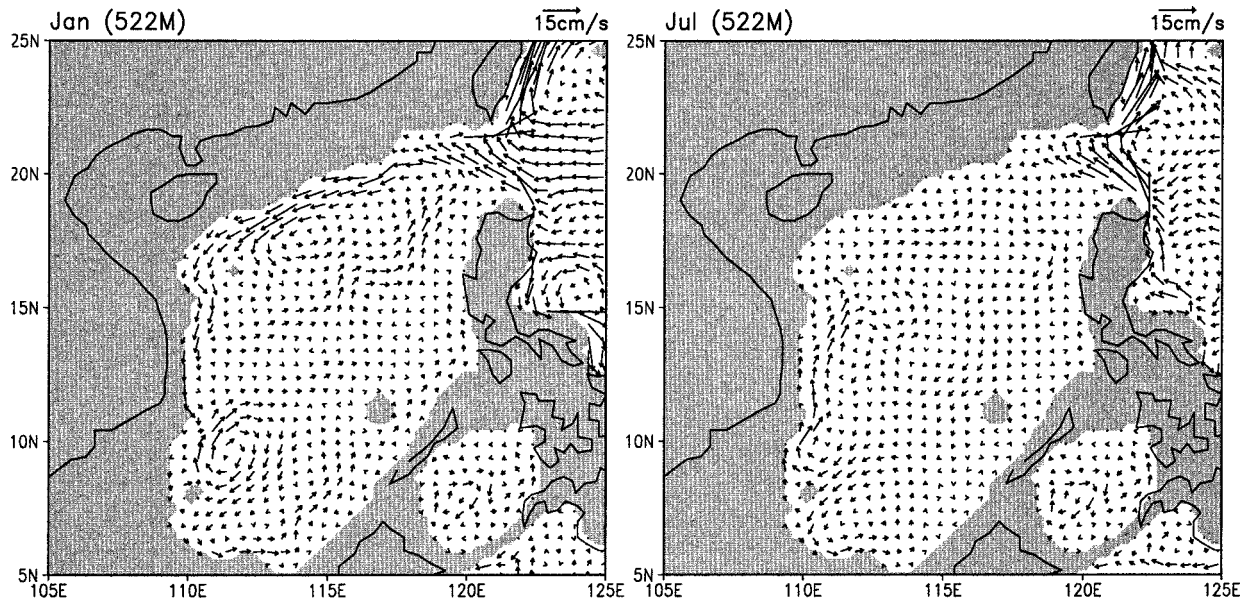
FIG. 3. As in Fig. 2 except at 522 m from the model.

heavy dotted line in Fig. 1) with the rest continuing westward (Fig. 5c).

Averaged along the section, the flow changes sign at about 400 m and becomes an outward flow below that depth, with a maximum speed occurring at about 500 m (Fig. 6, left). This result seems to agree with earlier observations (e.g., Wyrtki 1961; Qu et al. 2000), providing additional support for the assumption of a level of no motion at 400 m in the estimate of LST (Qu 2000). Several recent studies suggested that there is a sandwiched vertical structure in the mean LST; that is, an

FIG. 4. Annual mean streamfunction of total transport. Contours are 5 Sv for positive values and 2 Sv for negative values. An additional contour of −1 Sv is added.

outflow in the intermediate layer is accompanied by inflows in the upper and deeper layers (e.g., Chen and Huang 1996; Chao et al. 1996; Chen and Wang 1998; Qu 2002; Yuan 2002). This vertical structure is not shown in the present model, although interleaving inflows/outflows do exist below 400 m.

b. Seasonal variation

The vertical profile of LST (Fig. 6, left) contains a strong seasonal cycle (Fig. 6, right). In the upper 400 m, the flow is predominantly westward. Outflows are present near the surface only from June to September, when the southwest monsoon prevails, but appear to be a year-round phenomenon at about 500 m. Intermittent outflows are also seen around 900 m but are rather weak compared with those in the shallower waters. Below about 1500 m, the flow is dominated by an outflow component roughly from January to June and an inflow component during the rest of the year. Both components are of the order 1 Sv, thus leading to a net transport very close to zero. Although there is no observational evidence for this seasonal variation in the deep layers, the model results at least suggest that snapshot measurements of LST may not be representative around the sill depth of Luzon Strait.

The total transport through Luzon Strait has a maximum (6.1 Sv westward) in January and a minimum (0.9 Sv eastward) in June (Fig. 7a). A similar result is also shown for the upper-layer (0–405 m) transport except for a phase difference of 1–2 months in summer. These results are in remarkable agreement with the earlier observations of Qu (2000), who obtained a maximum transport of 5.3 Sv (westward) in January–Feb-
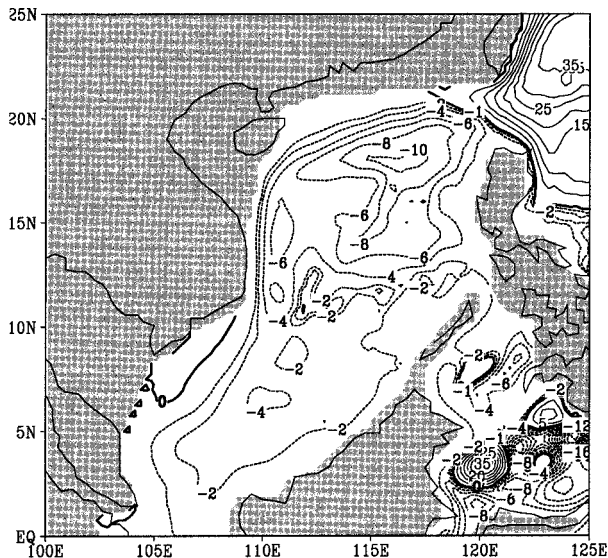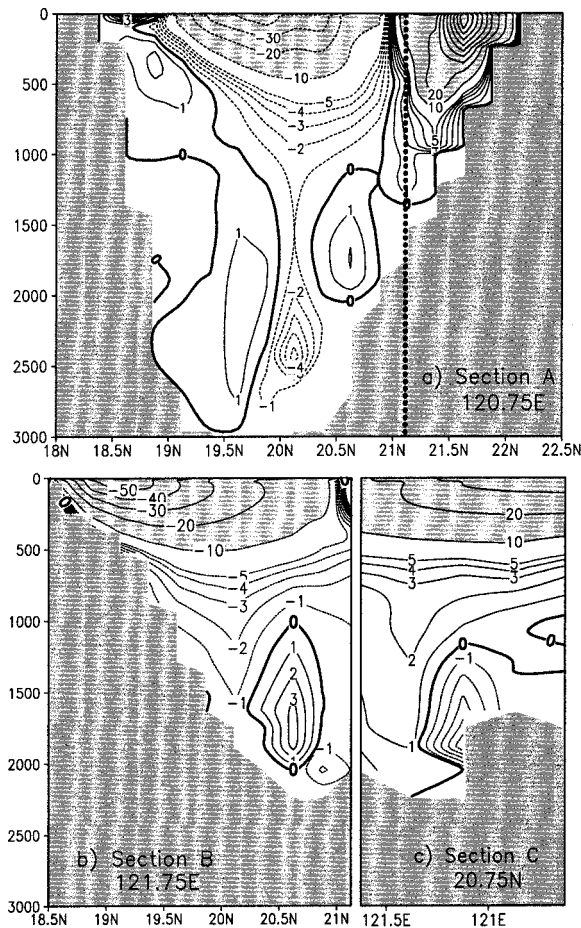
FIG. 5. Annual mean velocity (cm s⁻¹) across Luzon Strait at (a) 120.75°E, (b) 121.75°E, and (c) 20.75°N. Positive values indicate eastward flow in (a) and (b) and northward flow in (c). The heavy dotted line in (a) indicates the transect of section C on A. Contour intervals are 10 cm s⁻¹ for shaded areas and 1 cm s⁻¹ elsewhere. Geographic locations of these sections are shown in Fig. 1.

ruary and a minimum transport of 0.2 Sv (westward) in June–July (Fig. 7a), suggesting that the model does a good job in reproducing the seasonal variation of LST.

The volume transport across the Sunda Shelf is nearly in phase with LST (Fig. 7b), with a maximum (5.4 Sv southward) in January and a minimum (1.5 Sv northward) in June, showing good agreement with that reported by Lebedev and Yaremchuk (2000). The volume transport through Mindoro Strait is relatively weak, fluctuating between about 1.5 Sv (southward) in October and almost zero in April. The vertical transport at 405 m, as a consequence of mass balance, is downward from February to June and upward from July to January; its peak-to-peak amplitude is smaller by a factor about 3 than that of LST.

Although directly wind-driven circulation does not appear to make a significant contribution to the seasonal variation of LST, the piling up of water induced by the monsoonal winds is believed to be an important mech-

anism changing the pressure gradient across Luzon Strait and eventually affecting the LST (e.g., Metzger and Hurlburt 1996; Qu 2000; Lebedev and Yaremchuk 2000). Yaremchuk and Qu (2004) also attributed the seasonal variation of LST to the nonlinear hysteresis of the Kuroshio. According to Sheremet (2001), an inertial boundary current may leap across a gap in the western boundary when the meridional advection of potential vorticity is strong enough to overpower the β effect. As soon as the current's transport falls below a critical value (depending on the strait width, β, and horizontal and vertical scales of the current), the current will switch into a "gap penetrating" regime. Based on the results from a numerical model that incorporates drifter, satellite, and hydrographic data, Yaremchuk and Qu (2004) suggested that this critical value of the Kuroshio transport (KT) lies between 15 and 20 Sv.

The seasonal variation of LST seems to follow this rule and shows an opposite phase with that of the Kuroshio transport east of Luzon (Fig. 7c). During the northeast monsoon season, a cyclonic deviation from mean circulation occurs in the Philippine Sea, which shifts the NEC bifurcation northward (Qu and Lukas 2003) and consequently intensifies the Mindanao Dome and reduces the Kuroshio transport east of Luzon (Masumoto and Yamagata 1991; Tozuka et al. 2002; Yaremchuk and Qu 2004). When the Kuroshio transport approaches its seasonal minimum (~10 Sv) in November/December, water from the Pacific penetrates more easily into the SCS through Luzon Strait, causing a rapid increase in LST toward its seasonal maximum in January (Yaremchuk and Qu 2004). The situation is reversed during the southwest monsoon.

c. Interannual variation

Figure 8 shows the interannual variation of the LST relative to its mean seasonal cycle from January 1982 through December 1998. A 12-month moving average has been applied to remove higher frequency variations. During this whole period of time, the interannual variations of the LST in the upper 405 m and their total value (surface–bottom) are almost identical, with a correlation exceeding 0.90. For convenience, only the upper-layer (0–405 m) LST is discussed below.

The temporal correspondence of LST with ENSO is striking. The correlation between the LST and the Southern Oscillation index (SOI) reaches 0.63, with LST leading SOI by about 1 month (Table 1). In general, the LST is stronger during El Niño years (e.g., 1982–83, 1986–87, and 1997–98), and weaker during La Niña (e.g., 1984–85, 1988–89, and 1996–97). Its peak-to-peak amplitude is about 3 Sv, smaller than that of the seasonal cycle by a factor of about 2.5. This result implies that the seasonal variation associated with the monsoon is still the dominant signal in LST.

The interannual variation of the LST is also closely related to the Kuroshio transport east of Luzon (Fig.
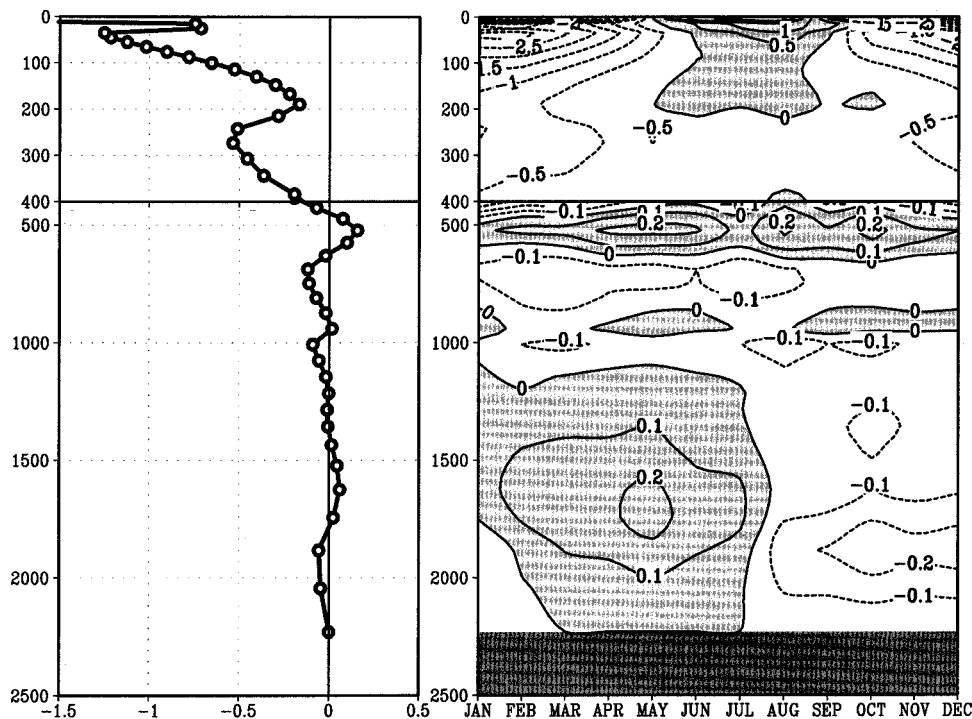
FIG. 6. Vertical distribution of the Luzon Strait transport (10^4 m^2 s^{-1}) against depth (m): (left) annual mean and (right) seasonal variation.

9), presumably in the same way as that discussed for the seasonal cycle (Yaremchuk and Qu 2004). The correlation between the LST and the upper-layer (0–405 m) Kuroshio transport reaches 0.56, with the maximum (westward) LST leading the minimum (northward) Kuroshio transport by about 4 months. If the total Kuroshio transport (surface–bottom) is considered, this correlation is slightly reduced (0.54). The interannual variation of the Kuroshio transport can be explained by the meridional migration of the NEC bifurcation (Kim et al. 2004). During El Niño years, the northward shift of the NEC bifurcation corresponds to a stronger Mindanao Dome and a weaker Kuroshio transport (Masumoto and Yamagata 1991; Tozuka et al. 2002), thus providing a favorable condition for Pacific waters to penetrate into the SCS through Luzon Strait. The situation is reversed during La Niña years (Yaremchuk and Qu 2004).

Transports across the Sunda shelf and Mindoro Strait show a similar interannual variation as the LST (Fig. 10), and their instantaneous correlations with LST reach 0.66 and 0.79, respectively (Table 1). In general, all the three transports are higher during El Niño years and lower during La Niña years. Vertical transport at 405 m, representing the deep-layer (below 405 m) component of LST, is relatively weak. Its correlation with the SCS wind stress curl is low (<0.2), indicating that local Ekman pumping is not an important driving mechanism.

5. SCS thermal balance

To understand the role of LST in the upper-layer (0–405 m) thermal balance of the SCS, it is helpful to write down the heat content conservation equation as follows (cf. Qu et al. 1994):

$$C_p \rho \iiint_{\text{SCS}} \frac{\partial \overline{T}}{\partial t} d\sigma = \overline{Q} + C_p \rho \iint_{A_l} \overline{v_n T} \, dA$$

$$+ C_p \rho \iint_{A_b} \overline{wT} \, dA + R. \quad (1)$$

Here A_l and A_b represent the lateral boundary and the horizontal surface of the lower boundary at 405 m, respectively. The independent variable t denotes time, T is temperature, v_n is the horizontal velocity component normal to the lateral boundary and w is vertical velocity, and ρ and C_p are the reference density and specific heat of seawater. The quantities with an overbar represent ensemble monthly mean values. In the following, we refer to the term on the left-hand side of (1) as heat content change (HCC), the first term on the right-hand side as surface heat flux Q, and the second and third terms as heat advection (Adv). The fourth term R on the right-hand side represents the parameterizations of subgrid-scale (<0.25°) mixing (described in section 2). Estimating subgrid-scale mixing requires instantaneous model outputs because of the strong nonlinearity of the Pacanowski and Philander (1981) parameterization. The
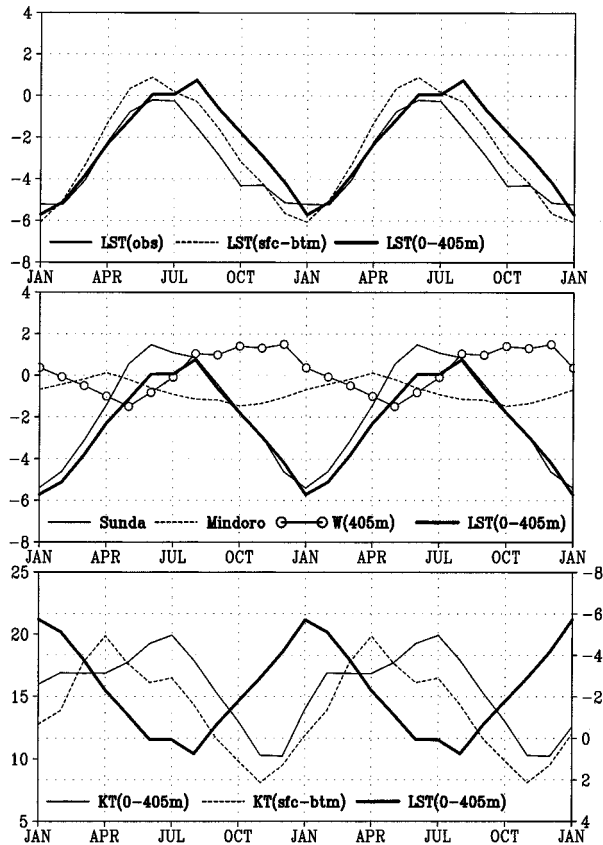
FIG. 7. Seasonal variations of the Luzon Strait transport at 120.75°E, the Sunda Shelf transport at 0.25°N, the Mindoro Strait transport at 11.25°N, the vertical transport at 405 m, and the Kuroshio transport east of Luzon at 18.25°N. (top) The LST from Qu's (2000) climatology is also included. (bottom) To show the nonlinear hysteresis of the Kuroshio, the axis for the LST is reversed. The unit is Sv.

instantaneous model outputs are not available for this study; consequently, the subgrid-scale mixing is simply calculated as the residual of the heat budget (called residual flux hereinafter).

Before proceeding further, we note that the selection of the lower boundary at 405 m was based mainly on two facts: First, most of the LST occurs in the upper 405 m (see section 4), and thus the vertical heat flux

TABLE 1. Correlation coefficients between LST (0–405 m) and the Sunda Shelf transport (ST), the Mindoro Strait transport (MST), the Kuroshio transport (KT) east of Luzon, and the SOI. All values are significant at 95% confidence level.

	ST	MST	KT (0–405 m)	KT (surface–bottom)	SOI
Correlation coefficient	0.66	0.79	0.56	−0.54	0.63
Time lag (month)	0	0	−4	−2	1

across 405 m is expected to be small. Second, this depth is well below the thermocline of the SCS, so the upper-layer (0–405 m) heat content change may have a reasonable representation of the variability in depth of the thermocline. Results of heat budget analysis in the upper 405 m are presented below.

a. Annual mean

All heat budget terms of Eq. (1) were calculated using ensemble monthly data from January 1982 to December 1998, and these values were then averaged to produce the annual mean values. Figure 11a shows the annual mean surface heat flux from the model. Overall, its spatial distribution agrees with Oberhuber's (1988) climatology (Fig. 11b). As already indicated in earlier studies (e.g., Qu 2001), the atmosphere heats the ocean in most parts of the SCS except for a small region over the continental shelf south of China, where surface cooling reaches −60 W m^{-2}. Averaged over the entire basin of the SCS, the annual mean surface heat flux from the model is 17 W m^{-2}, slightly smaller than Oberhuber's climatology (23 W m^{-2}). Given that the SCS is essentially semiclosed (Fig. 1), most of the heat gain from the atmosphere has to be counterbalanced by heat advection through Luzon Strait and several shallow passages in the south, namely, the Sunda shelf and Mindoro Strait. To examine the exact role of LST in the SCS thermal balance is the main object of this paper.

On average, water enters the SCS in the upper 405 m with a lower temperature (21.6°C) through Luzon Strait and leaves it with higher temperatures (26.5° and
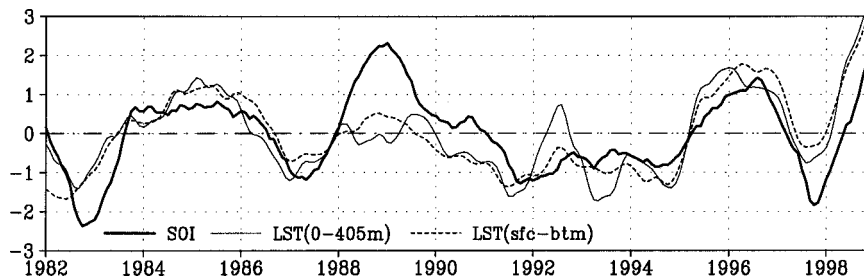

FIG. 8. Interannual variations of LST and the Southern Oscillation index (SOI) normalized by their respective rms variance. Rms variance is 0.68 Sv for LST (0–405 m), 0.65 Sv for LST (surface–bottom), and 0.77 for SOI.
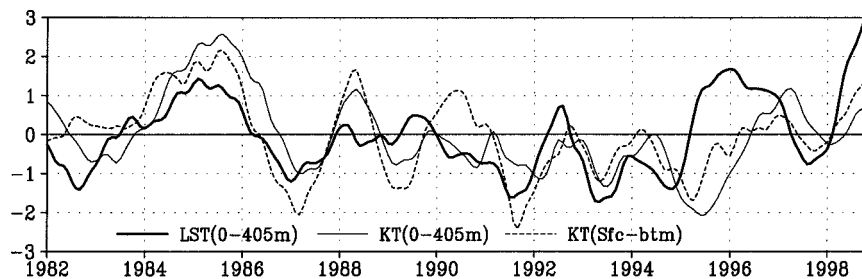
FIG. 9. As in Fig. 8 except for the Kuroshio transport off Luzon at 18.25°N. Rms variance is 2.8 Sv for KT (0–405 m) and 5.4 Sv for KT (surface–bottom).

27.5°C) over the shallow (<200 m) Sunda Shelf and Mindoro Strait (Table 2). As such, horizontal circulation accomplishes a cooling advection of -54.5×10^{12} W. Vertical transport in the mean is very close to zero (<0.01 Sv) at 405 m, but the net heat flux across this depth can still reach -4.9×10^{12} W, accounting for about 8% of the total heat advection (-59.4×10^{12} W, Table 3). With a surface area of 3.1×10^{12} m^2 in the SCS, the total heat advection is equivalent to a surface heat flux of -19 W m^{-2}. Surface heat flux is the primary heating process and balances about 86% of the advective cooling. The residual heat flux slightly heats the ocean at a rate of about 4 W m^{-2}. In the upper layer of Luzon Strait, there is a large temperature gradient (Fig. 12). At a fixed level within the depth range of the thermocline, the annual mean temperature on the SCS side is lower by as much as 2°C than that on the Pacific side, indicating that the Kuroshio carries relatively warm water into the SCS. With this temperature gradient, one can easily expect a net heat flux from the Pacific into the SCS as a result of subgrid-scale mixing parameterized by a scale-selective biharmonic operator in the model (Ishida et al. 1998). It must be noted, however, that as water leaving the SCS in the south is of even higher temperature than that with the Kuroshio, heat advection and mixing together play a negative role in the annual-mean heat balance of the SCS (Table 3). Another important contribution (~ 1 W m^{-2}) to the residual heat flux is due to heat content change. A perfect annual-mean heat budget would require the integrated heat content change to be zero. It is not exactly zero in

Table 3 because of interannual variations and possible background model drift.

In section 4 we have noted that closing Taiwan Strait may reduce the LST in the model. Can this reduction in the LST, if any, influence the SCS thermal balance? To gain insight into this question, we have examined the Levitus (1982) climatological data and found that the annual mean temperature in Taiwan Strait (<100 m) is not much different from that in the upper layer of Luzon Strait. At 24.5°N, for example, the annual mean temperature along the section is 22.2°C, only about 0.6°C higher than that (21.6°C) shown in Table 2 for LST but much lower than those (27.5° and 26.5°C) for Shunda shelf transport (ST) and Mindoro Strait transport (MST). As such, closing Taiwan Strait in the model does not appear to have a significant influence on the SCS thermal balance.

b. Seasonal variation

The upper-layer heat content (HC405 hereinafter) in the SCS shows essentially the same seasonal cycle as SST except for a phase difference in summer (Fig. 13). On average, SST has a maximum in June and decreases in subsequent months with the development of the southwest monsoon, while HC405 reaches its seasonal maximum in September. This difference in phase reflects the strong influence of mixed layer dynamics on SST. From late spring to early summer, as mixed layer depth (MLD) shoals against the diminishing northeast monsoon, heat gained from the atmosphere is trapped
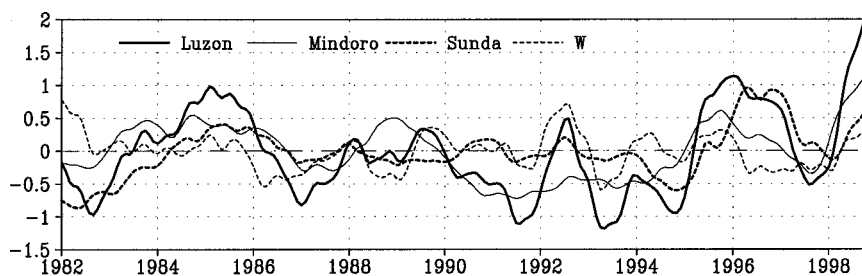

FIG. 10. Interannual variations of the Sunda Shelf transport at 0.25°N, the Mindoro Strait transport at 11.25°N, and the vertical transport at 405 m.
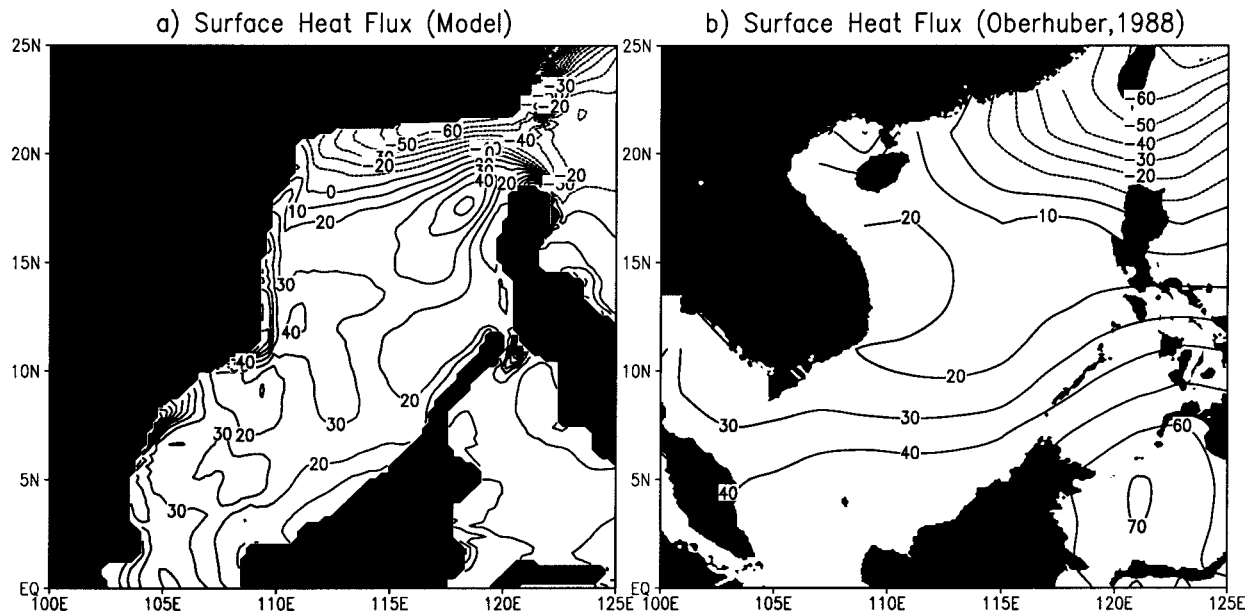
FIG. 11. Annual mean surface heat flux (W m^{-2}) from (a) the model and (b) Oberhuber's (1988) climatology.

in a shallower mixed layer, and this eventually warms the sea surface in the SCS (Qu 2001). Deepening of the mixed layer forced by the southwest monsoon marks the end of this heat accumulation, thus giving rise to a decrease of SST in subsequent months despite the incoming surface heat flux. The vertical redistribution of heat associated with the seasonal thermocline in summer, however, has little effect on the upper-layer heat content. HC405 continues to increase until the surface heat flux changes sign in September/October (Fig. 14).

The seasonal heat content change in the upper 405 m is large, ranging from about 200×10^{12} in May to about -200×10^{12} W in December, and can be explained mostly by surface heat flux and heat advection (Fig. 14). On average, the surface heat flux is positive from January to October, with a maximum exceeding 130×10^{12} W in April, and slightly negative ($\sim -30 \times 10^{12}$ W) in November/December. Heat advection slightly heats the SCS from April to July, when both

LST and ST tend to change their directions (Fig. 7), but cools it intensively during the rest of the year. The peak-to-peak amplitude of heat advection exceeds 280×10^{12}, larger by a factor of about 2 than that of surface heat flux. In winter, the cooling by heat advection reaches about -200×10^{12} W, accounting for nearly 90% of the upper-layer heat content change. This cooling is apparently associated with the seasonal maximum of LST (Fig. 7b), though Ekman pumping forced by the northeast monsoon at that season may also play a role (Qu 2000). The residual heat flux does not change significantly throughout the year, suggesting that small-scale eddies and subgrid-scale processes have little effect on the seasonal variation of HC405.

c. Interannual variation

The temporal correspondence between SST and ENSO in the SCS has been reported by several earlier studies (e.g., Ose et al. 1997; Wang et al. 1997, 2000, 2002; Xie et al. 2003). According to these studies, SST gets warmer in the SCS during and after the mature phase of El Niño, presumably as a result of interaction between an anomalous atmospheric anticyclonic circulation and the ocean mixed layer dynamics. Here, we find that the overall correlation between the SCS SST and SOI is -0.36, with SOI leading the SST by about 7 months (Fig. 15). This result clearly indicates that the warm SCS SST anomaly that appears during the mature phase of El Niño (Wang et al. 1997) peaks in the following summer. If only December SOI and July SST data are used, the correlation increases to -0.49, satisfying the 95% confidential level criterion. Spatially, the correlation between SST and SOI is negative all

TABLE 2. Annual mean mass budgets for all, El Niño, and La Niña years. El Niño years include 1982, 1986, 1991, 1994, and 1997, and La Niña years include 1984, 1988, and 1996. Positive values indicate eastward for the LST and northward for Sunda Shelf transport (ST) and Mindoro Strait transport (MST).

	LST	ST	MST
	Transport (Sv)		
All	-2.4	-1.7	-0.7
El Niño	-3.1	-2.0	-1.1
La Niña	-2.1	-1.4	-0.5
	Temperature (°C)		
All	21.6	27.5	26.5
El Niño	21.0	27.2	26.4
La Niña	21.2	26.5	27.5

TABLE 3. Annual mean heat budgets for all, El Niño, and La Niña years. HCC denotes heat content change in the upper 405 m, Q surface heat flux, Adv heat advection, and R residual heat flux.

	HCC (10^{12} W)	Q (10^{12} W)	Adv (10^{12} W)	R (10^{12} W)
All	3.4	51.2	−59.4	11.6
El Niño	−10.8	55.0	−77.6	11.8
La Niña	22.4	44.7	−30.7	8.4

over the SCS, and this forms a sharp contrast with the positive correlation in the tropical western Pacific (Fig. 16), reflecting different SST formation mechanisms in the two regions. The importance of this difference in the development of El Niño has been noted by earlier studies (e.g., Yamagata and Masumoto 1989; Masumoto and Yamagata 1991). Prior to El Niño, SST is warmer in the tropical western Pacific and cooler in the SCS, and this induces a sea surface pressure difference between the two regions, which invites more cold surges (westerly bursts) and provides a trigger of El Niño.

In many parts of the global ocean, SST heavily depends on the MLD, and a higher SST usually corresponds to a deeper MLD and consequently a larger upper-layer heat storage. In the eastern equatorial Pacific (5°S–5°N, 150°–90°W), for example, the correlation between SST and HC405 in the model reaches 0.92. This, however, does not seem to be the case in the SCS, presumably due to the presence of a seasonal thermocline (Qu 2001), where the correlation between SST and HC405 drops to 0.58 (Fig. 15). If the extreme 1997–98 event is excluded, this correlation is only 0.20 for the entire basin, as one would expect from the time series shown in Fig. 15, but can reach 0.55 in the northern part of the SCS (north of 14°N). This result implies that, although the correlation is relatively low compared with many parts of the global ocean (e.g., the eastern equatorial Pacific), HC405 is still an important proxy of SST in the SCS. A better understanding of the interannual

variation in HC405 is essential for future studies of the SCS climate. We will focus on the interannual variation of HC405 in the following discussions.

Over the entire basin of the SCS, HC405 has a minimum around the mature phase of El Niño, and its correlation with SOI reaches 0.46. As a consequence, the upper-layer heat content change also shows a good correspondence with ENSO. Its correlation with SOI reaches 0.45 with HCC leading SOI by about 5 months (Fig. 17). At the developing stage of El Niño (e.g., 1982, 1991, and 1997) HCC is negative, indicative of a decrease in HC405. HCC becomes positive as El Niño starts to decay, and a warming in HC405 seems to be a common feature to most of the La Niña events (e.g., 1984, 1988, and 1996). The exceptions, like those occurring in 1986 and 1993, might be interpreted as evidence that, in addition to ENSO, the upper-layer heat content in the SCS is also affected by other processes. But, in general, the effect of ENSO is evident.

Heat budget analysis suggests that heat advection is the most important factor determining the upper-layer heat content change in the SCS (Fig. 17). The instantaneous correlation between HCC and heat advection exceeds 0.8 (Table 4). The correlation between HCC and surface heat flux is not significant (−0.20). But, adding surface heat flux better explains the upper-layer heat content change, and the correlation between HCC and the sum of surface heat flux and heat advection reaches as high as 0.96. The residual heat flux is generally small, suggesting that small-scale eddies and subgrid-scale processes play little role in the interannual heat balance of the SCS.

How can ENSO affect the upper-layer heat content in the SCS? In section 4c, we have noted that the in-
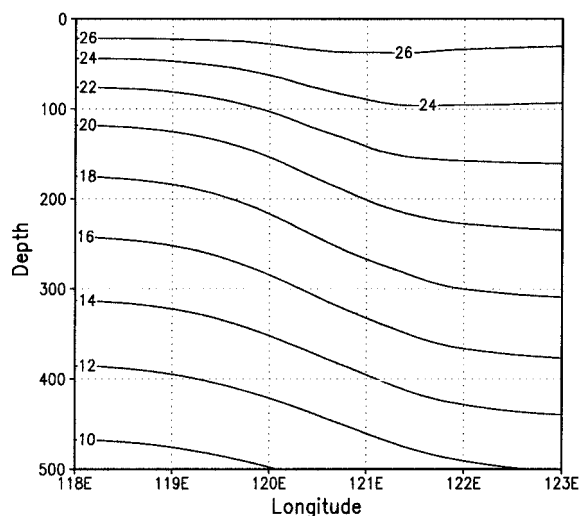

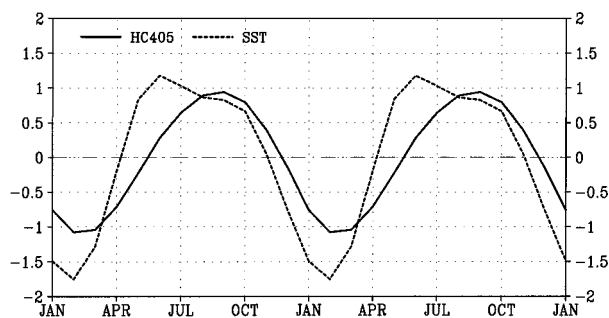FIG. 12. Annual mean temperature (°C) across Luzon Strait at 20.625°N.

FIG. 13. Seasonal variations of SST (°C) and upper-layer (0–405 m) heat content (10^{21} cal). The annual mean values of 27.8°C for SST and 56.9 × 10^{21} cal for heat content have been subtracted before plotting.
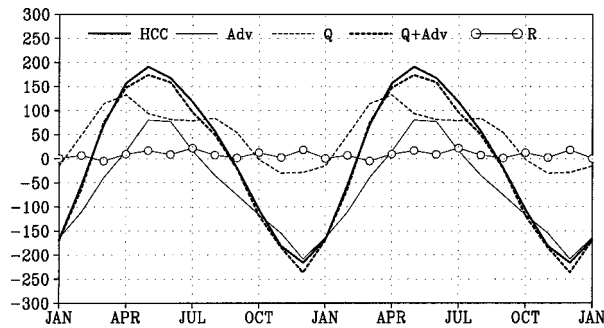
FIG. 14. Seasonal heat budget in the upper 405 m of the SCS. The unit is 10^{12} W.

FIG. 16. Correlation coefficient between SST and SOI, with SOI leading SST by 7 months.

terannual variation of LST contains a strong ENSO signal. With this ENSO signal in LST, the correlation between heat advection and SOI is high, exceeding 0.62 with heat advection leading SOI by 3 months (Table 4). At the developing stage of El Niño (e.g., 1982, 1991, and 1997), LST increases toward its maximum strength, and this produces a stronger than normal cooling advection, which eventually cools the upper-layer of the SCS (Fig. 17). The situation seems to be reversed at the developing stage of La Niña (e.g., 1984, 1988, and 1996).

It is worthwhile to note that there is a phase difference between LST (0–405 m) and heat content change in the SCS. The maximum cooling in the upper layer of the SCS occurs 4 months earlier than the maximum LST or 5 months earlier than the mature phase of El Niño. Surface heat flux, which is negatively correlated with heat advection (Table 4), apparently contributes to this phase difference. If only heat advection is considered (i.e., Adv vs LST), this phase difference is reduced to only 2 months. In addition to the ensemble effect of small-scale eddies and subgrid-scale processes, the lead of heat advection to LST (0–405 m) could also be a result of vertical heat flux across 405 m, indicative of the importance of deep-water exchange between the SCS and the Pacific through Luzon Strait in the upper-layer thermal balance of the SCS.

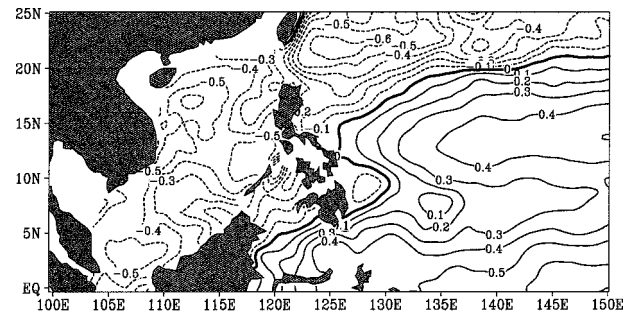As an example, Tables 2 and 3 show a composite of the annual mean mass and heat budgets for all El Niño and La Niña events that occurred during the period from 1982 to 1998. Here, only the developing stages of these events (i.e., 1982, 1986, 1991, 1994, and 1997 for El Niño events and 1984, 1988, and 1996 for La Niña events) are considered. As El Niño develops, the annual mean LST is stronger than normal by 0.7 Sv, and the heat advection reaches -77.6×10^{12} W. Surface heat flux only slightly increases during these events, and the enhanced heat advection induces a cooling (-10.8×10^{12} W) in the upper-layer heat content, equivalent to a surface heat flux of about -4 W m^{-2} over the entire basin of the SCS. The cooling advection becomes weaker when El Niño starts to decay and falls below -30.1×10^{12} W at the developing stage of La Niña. Part ($\sim$22%) of this anomaly in heat advection is balanced by the weakening in surface heat flux, and the rest produces a warming (22.4 $\times 10^{12}$ W) in the upper layer of the SCS.

6. Summary and discussion

Based on the results from a high-resolution ocean general circulation model, this study provides a detailed description of the Luzon Strait transport and its role in the South China Sea thermal balance. The results are summarized as follows.

The annual mean LST from the model is 2.4 Sv, which compares quite favorably with existing observations. Most of this transport is confined in the upper 405 m. Though water exchange does occur in the deeper layers, the net transport below 405 m is negligibly small.
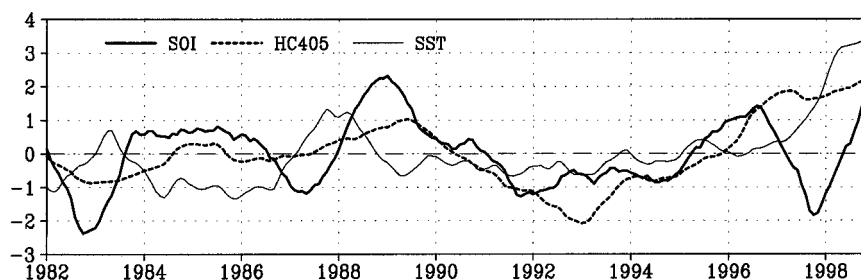

FIG. 15. Interannual variations of SST, HC405, and SOI normalized by their respective rms variance. Rms variance is 0.3°C for SST, 4.67 $\times 10^{20}$ cal for HC405, and 0.77 for SOI.
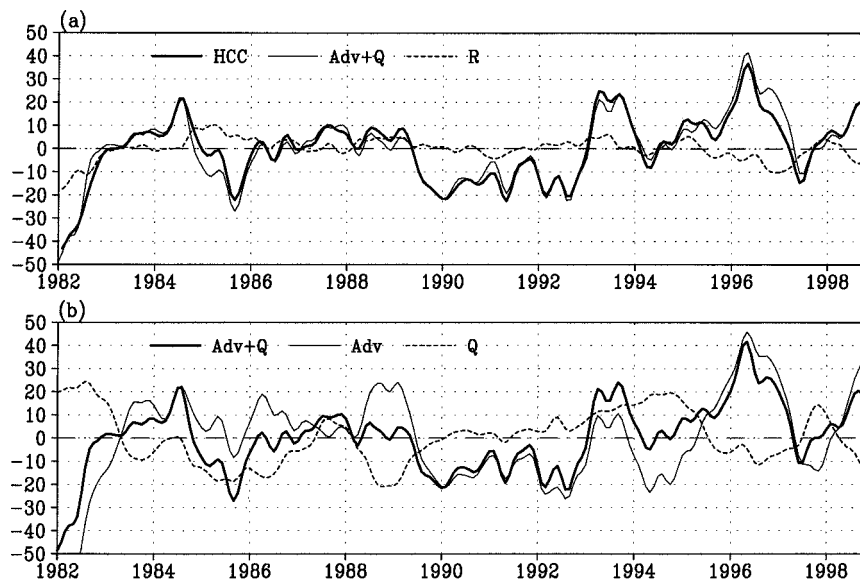
FIG. 17. As in Fig. 14 except for interannual variations.

This provides additional support for the assumption of a reference level at 400 m in the estimate of LST.

The model has a good representation of the seasonal variation of LST, showing a maximum (6.1 Sv westward) in winter and a minimum (0.9 Sv eastward) in summer. On an interannual time scale, LST tends to be larger during El Niño years and smaller during La Niña years, and its correlation with SOI exceeds 0.63. In addition to the monsoonal winds, the variation of LST may also be attributed to nonlinear hysteresis of the Kuroshio.

For the annual average, temperature on the Pacific side is higher than that on the SCS side of Luzon Strait, indicating that the Kuroshio carries relatively warm water into the SCS. However, as water leaving the SCS in the south is of even higher temperature, heat advection plays a negative role in the SCS annual mean thermal balance. In the upper 405 m, the annual-mean heat advection is equivalent to a surface heat flux of -19

TABLE 4. Correlation coefficients between upper-layer (0–405 m) HCC, Q, Adv, the sum of surface heat flux and heat advection (Q + Adv), and SOI. Values satisfying the 95% confidence level criterion are in boldface.

	Q	Adv	Q + Adv	SOI
HCC (0–405 m)				
Correlation coefficient	−0.2	**0.81**	**0.96**	**0.45**
Time lag (month)	0	0	0	−5
Adv				
Correlation coefficient	**−0.66**	**1.0**	**0.83**	**0.62**
Time lag (month)	−1	0	0	−3

W m^{-2}, most of which is balanced by surface heat flux (17 W m^{-2}) and the rest by the residual heat flux representing the influence of small-scale eddies and subgrid-scale processes.

Both surface heat flux and heat advection are fundamental to the seasonal variation of the upper-layer heat content. From late spring to early fall, surface heat flux is the primary heating process; only a small part of the heat content change can be explained by heat advection. In winter, heat advection seems to be the only important process responsible for the cooling in the upper layer of the SCS. The strong cooling advection in winter is associated with the seasonal maximum of LST.

The interannual variation of the upper-layer heat content shows good temporal correspondence with ENSO. In most cases, maximum cooling occurs earlier, by about 5 months, than the mature phase of El Niño. Upper-layer heat content becomes warmer as El Niño decays, and the warming persists into the developing stage of La Niña. This variation can be largely explained by heat advection, although the effect of surface heat flux is not negligible.

The interannual variation of SST also shows good correspondence with ENSO but has a different phase with that of the upper-layer heat content. SST increases around the mature phase of El Niño and peaks in the following summer. Using atmospheric data, earlier studies have suggested that surface heat flux is the primary forcing mechanism for SST variability, but the precise role of ocean dynamics has never been carefully examined because of the lack of oceanographic data. This study provides the first evidence to suggest that horizontal heat advection is a key factor influencing the upper-layer heat content. Left to be addressed for future studies is a detailed mixed layer heat budget to better identify the role of ocean dynamics in SST variability of the SCS.

Finally, we note that the LST is an important process conveying the impact of ENSO to the SCS. This oceanic connection has been ignored by earlier studies. We believe that its revelation will be useful for future studies of the SCS climate.

REFERENCES

Broecker, W. S., W. C. Patzert, J. R. Toggweiler, and M. Stuvier, 1986: Hydrography, chemistry, and radioisotopes in the southeast Asian basin. *J. Geophys. Res.,* **91,** 14 345–14 354.

Chao, S.-Y., P.-T. Shaw, and S. Y. Wu, 1996: Deep sea ventilation in the South China Sea. *Deep-Sea Res.,* **43A,** 445–466.

Chen, C.-T., and M. H. Huang, 1996: A mid-depth front separating the South China Sea water and the Philippine Sea water. *J. Oceanogr.,* **52,** 17–25.

——, and S.-L. Wang, 1998: Influence of the intermediate water in the western Okinawa Trough by the outflow from the South China Sea. *J. Geophys. Res.,* **103,** 12 683–12 688.

Chu, P. C., and R. Li, 2000: South China Sea isopycnal-surface circulation. *J. Phys. Oceanogr.,* **30,** 2419–2438.

Fang, G., B. Zhao, and Y. Zhu, 1991: Volume transport through the Taiwan Strait and the continental shelf of the East China Sea measured with current meters. *Oceanography of Asian Marginal Seas,* K. Takano, Ed., Elsevier Oceanography Series, Vol. 54, Elsevier, 345–358.

Godfrey, J. S., 1989: A Sverdrup model of the depth-integrated flow for the world ocean allowing for island circulations. *Geophys. Astrophys. Fluid Dyn.,* **45,** 89–112.

Guo, Z., 1985: Wintertime South China Sea Warm Current and the westward current on its right (in Chinese with English abstract). *Trop. Oceanol.,* **4,** 1–9.

Hellerman, S., and M. Rosenstein, 1983: Normal monthly wind stress over the world ocean with error estimates. *J. Phys. Oceanogr.,* **13,** 1093–1104.

Ishida, A., Y. Kashino, H. Mitsudera, N. Yoshioka, and T. Kadokura, 1998: Preliminary results of a global high-resolution GCM experiment. *J. Fac. Sci. Hokkaido Univ. Ser. 7,* **11,** 441–460.

Kim, Y. Y., T. Qu, T. Jensen, T. Miyama, H.-W. Kang, H. Mitsudera, and A. Ishida, 2004: Seasonal and interannual variations of the North Equatorial Current bifurcation in a high-resolution OGCM. *J. Geophys. Res.,* **109,** C03040, doi:10.1029/2003JC002013.

Lebedev, K. V., and M. I. Yaremchuk, 2000: A diagnostic study of the Indonesian Throughflow. *J. Geophys. Res.,* **105,** 11 243–11 258.

Levitus, S., 1982: *Climatological Atlas of the World Ocean.* NOAA Prof. Paper 13, 173 pp. and 17 microfiche.

Masumoto, Y., and T. Yamagata, 1991: Response of the western tropical Pacific to the Asian winter monsoon: The generation of the Mindanao Dome. *J. Phys. Oceanogr.,* **21,** 1386–1398.

Metzger, E. J., and H. E. Hurlburt, 1996: Coupled dynamics of the South China Sea, the Sulu Sea, and the Pacific Ocean. *J. Geophys. Res.,* **101,** 12 331–12 352.

Nitani, H., 1972: Beginning of the Kuroshio. *Kuroshio: Physical Aspects of the Japan Current,* H. Stommel and K. Yoshida, Eds., University of Washington Press, 129–163.

Oberhuber, J. M., 1988: An atlas based on the ''COADS'' data set: The budgets of heat, buoyancy and turbulent kinetic energy at the surface of the global ocean. Rep. 15, Max Planck Institut fur Meteorologie, Hamburg, Germany.

Ose, T., Y. Song, and A. Kitoh, 1997: Sea surface temperature in the South China Sea: An index for the Asian monsoon and ENSO system. *J. Meteor. Soc. Japan,* **75,** 1091–1107.

Pacanowski, R. C., and S. G. H. Philander, 1981: Parameterization of vertical mixing in numerical models of tropical oceans. *J. Phys. Oceanogr.,* **11,** 1443–1451.

Qiu, D., T. Yang, and Z. Guo, 1984: A westward current in the northeastern part of the South China Sea (in Chinese with English abstract). *Trop. Oceanol.,* **33,** 65–73.

Qu, T., 2000: Upper-layer circulation in the South China Sea. *J. Phys. Oceanogr.,* **30,** 1450–1460.

——, 2001: Role of ocean dynamics in determining the mean seasonal cycle of the South China Sea surface temperature. *J. Geophys. Res.,* **106,** 6943–6955.

——, 2002: Evidence for water exchange between the South China Sea and the Pacific Ocean through the Luzon Strait. *Acta Oceanol. Sin.,* **21,** 175–185.

——, and R. Lukas, 2003: The bifurcation of the North Equatorial Current in the Pacific. *J. Phys. Oceanogr.,* **33,** 5–18.

——, G. Meyers, J. S. Godfrey, and D. Hu, 1994: Ocean dynamics in the region between Australia and Indonesia and its influence on the variation of sea surface temperature in a global general circulation model. *J. Geophys. Res.,* **99,** 18 433–18 445.

——, H. Mitsudera, and T. Yamagata, 2000: Intrusion of the North Pacific waters into the South China Sea. *J. Geophys. Res.,* **105,** 6415–6424.

——, S.-P. Xie, H. Mitsudera, and A. Ishida, 2002: Subduction of the North Pacific mode waters in a global high-resolution GCM. *J. Phys. Oceanogr.,* **32,** 746–763.

Shaw, P.-T., 1991: Seasonal variation of the intrusion of the Philippine Sea water into the South China Sea. *J. Geophys. Res.,* **96,** 821–827.

Sheremet, V., 2001: Hysteresis of a western boundary current leaping across a gap. *J. Phys. Oceanogr.,* **31,** 1247–1259.

Tomita, T., and T. Yasunari, 1996: Role of the northeast winter monsoon in the biennial oscillation of the ENSO/monsoon system. *J. Meteor. Soc. Japan,* **74,** 399–413.

Tozuka, T., T. Kagimoto, Y. Masumoto, and T. Yamagata, 2002: Simulated multiscale variations in the western tropical Pacific: The Mindanao Dome revisited. *J. Phys. Oceanogr.,* **32,** 1338–1359.

Wang, B., R. Wu, and X. Fu, 2000: Pacific–East Asian teleconnection: How does ENSO affect East Asian climate? *J. Climate,* **13,** 1517–1536.

Wang, D. X., F. Z. H. Qin, and X. Zhou, 1997: Study on air–sea interaction on the interannual timescale in the South China Sea (in Chinese). *Acta Meteor. Sin.,* **55,** 33–42.

Wang, J., 1986: Observation of abyssal flows in the northern South China Sea. *Acta Oceanogr. Taiwan.,* **16,** 36–45.

Wang, Q., Q. Liu, R. Hu, and Q. Xie, 2002: A possible role of the South China Sea in ENSO cycle. *Acta Oceanol. Sin.,* **21,** 217–226.

Wyrtki, K., 1961: Physical oceanography of the southeast Asian waters. Naga Rep. 2, Scripps Institution of Oceanography, La Jolla, CA, 195 pp.

Xie, S.-P., Q. Xie, D. Wang, and W. T. Liu, 2003: Summer upwelling in the South China Sea and its role in regional climate variations. *J. Geophys. Res.,* **108,** 3261, doi:10.1029/2003JC001867.

Yamagata, T., and Y. Masumoto, 1989: A simple ocean–atmosphere coupled model of the origin of a warm ENSO event. *Philos. Trans. Roy. Soc. London,* **329,** 225–236.

——, and S. K. Behera, 2001: Dynamics of ocean circulation in the South China Sea (in Japanese). *Ocean Dev. News,* **29,** 25–30.

Yaremchuk, M., and T. Qu, 2004: Seasonal variability of the large-scale currents near the coast of the Philippines. *J. Phys. Oceanogr.,* **34,** 844–855.

Yuan, D., 2002: A numerical study of the South China Sea deep circulation and its relation to the Luzon Strait transport. *Acta Oceanol. Sin.,* **21,** 187–202.

Zhang, R., A. Sumi, and M. Kimoto, 1996: Impact of El Niño on the East Asian monsoon: A diagnostic study of the '86/87 and '91/92 events. *J. Meteor. Soc. Japan,* **74,** 49–62.